HHS Public Access

Author manuscript

Science. Author manuscript; available in PMC 2020 March 03.

Published in final edited form as:

Science. 2019 May 03; 364(6439): . doi:10.1126/science.aat6982.

A compact synthetic pathway rewires cancer signaling to therapeutic effector release

Hokyung K. Chung[1,2,5], **Xinzhi Zou**[4], **Bryce T. Bajar**[4,5], **Veronica R. Brand**[4,5], **Yunwen Huo**[2,4,5], **Javier F. Alcudia**[3], **James E. Ferrell Jr**[6], **Michael Z. Lin**[2,4,5,6]

[1]Department of Biology, Stanford University, Stanford, California, USA

[2]Department of Neurobiology, Stanford University, Stanford, California, USA

[3]Neuroscience Gene Vector and Virus Core, Stanford University, Stanford, California, USA

[4]Department of Bioengineering, Stanford University, Stanford, California, USA

[5]Department of Pediatrics, Stanford University, Stanford, California, USA

[6]Department of Chemical and Systems Biology, Stanford University, Stanford, California, USA

Abstract

An important goal in synthetic biology is to engineer biochemical pathways to address unsolved biomedical problems. One long-standing problem in molecular medicine is the specific identification and ablation of cancer cells. Here, we describe a method named Rewiring of Aberrant Signaling to Effector Release (RASER), where oncogenic ErbB receptor activity, instead of being targeted for inhibition as in existing treatments, is co-opted to trigger therapeutic programs. RASER integrates ErbB activity to specifically link oncogenic states to the execution of desired outputs. A complete mathematical model of RASER and modularity in design enable rational optimization and output programming. Using RASER, we induced apoptosis and CRISPR/Cas9-mediated transcription of endogenous genes specifically in ErbB-hyperactive cancer cells. Delivery of apoptotic RASER by adeno-associated virus selectively ablated ErbB-hyperactive cancer cells while sparing ErbB-normal cells. RASER thus introduces a new concept for oncogene-specific cancer detection and treatment.

*Correspondence to: mzlin@stanford.edu.

Author contributions: H.K.C. designed and optimized the RASER system, revised and optimized the mathematical model, performed mammalian cell experiments, analyzed data, and wrote the manuscript. X.Z., Y.H., and V.R.B. performed mammalian cell experiments. B.T.B. developed the initial mathematical model. J.E.F. provided advice on the mathematical model. M.Z.L. conceived the RASER system, conceived and assisted with developing the mathematical model, wrote the manuscript, and provided supervision and advice. Author information: The authors declare no competing financial interests.

Supplementary Materials:
Materials and Methods
Supplementary Text
Figures S1-S14
References (*51 – 61*)

Competing interests: The authors declare no competing interests.

Data and materials availability: The nucleotide sequences of bicistronic cDNAs encoding ErbB-RASER1N-OFP, ErbB-RASER1C-OFP, ErbB-RASER1C-OFPBidBH3, ErbB-RASER1N-VPRdCas9, and ErbB-RASER1C-dCas9VP64, have been deposited into GenBank with the accession codes MK801285, MK801286, MK801287, and MK801288. MATLAB code used in this study is available from the corresponding authors upon request.

One Sentence Summary:

RASER is a rationally designed synthetic pathway that specifically detects an intracellular oncogenic state and rewires it to programmable therapeutic outputs.

Synthetic biology, the engineering of new functions into living cells, has the potential to produce novel solutions to difficult medical problems (1). One challenging problem is the specific identification and treatment of cancer cells. Cancer cells differ fundamentally from normal cells in constitutively activating signaling pathways promoting cell growth, proliferation, or survival (2). For example, constitutive activation of ErbB-family receptor tyrosine kinases (RTKs), which include ErbB1 (HER1, EGFR) and ErbB2 (HER2, Neu), occurs in a substantial fraction of brain, esophageal, head and neck, lung, and breast cancers (3). Treatments have been developed that are specific for ErbB receptors, but not for their constitutive state. These treatments, which include small-molecule drugs (4), antibodies (4), viruses (5), and cells (6), attempt to inhibit ErbB receptors or eliminate the cells expressing them. However, because ErbB receptors are also required in normal cells for physiological signaling (Fig. 1A), they cannot be fully inhibited, or the cells expressing them completely eliminated, without causing toxicity to healthy tissues.

We considered a new principle for cancer therapy where oncogenic signaling is not blocked but instead is detected and then co-opted to trigger therapeutic responses via signal rewiring (Fig. 1B). We propose that synthetic proteins could be introduced into cells to query the state of a specific signaling pathway and execute a therapeutic program only if an oncogenic state is detected, preventing undesired toxicities in normal tissues. For therapeutic versatility, the ability to activate any introduced protein or transcribe any gene of choice would be ideal. While signaling pathways have been engineered within immune cells to customize responses upon binding antigens enriched on cancer cells (7–9), the approach we propose would be conceptually different in sensing and rewiring oncogenic signals within cancer cells, targeting the fundamental biological difference between cancer and normal cells (10).

In this study, we report a synthetic system, composed of only two modular proteins, that functions as a molecular integrator to discern oncogenic ErbB signals from normal signals. The simplicity of this system, named Rewiring of Aberrant Signaling to Effector Release (RASER), allowed its behavior to be comprehensively simulated by a mathematical model, facilitating rational optimization. We demonstrate that RASER is more dependent on constitutive ErbB signaling than native growth- and survival-promoting kinase pathways, and can be easily programmed to produce a variety of therapeutic outputs, including apoptosis and transcription of endogenous genes. RASER represents the first method to detect a specific oncogenic signal in living cells, and may enable precision molecular therapeutics for cancer.

A simple synthetic system for rewiring aberrant signaling to effector release

An ideal system for linking oncogenic signal transduction to therapeutic outputs would have to meet two general requirements. First, it should be specific; *i.e.* it should differentiate

oncogenic signaling from normal signaling (fig. S1A). Second, it should be programmable; *i.e.* it should be able to convert the presence of an oncogenic signal to a variety of therapeutic outputs. For the first requirement, we considered that oncogenic signaling is constitutive and so signal integration over time should produce a measurement specific for cancer states. For the second requirement, we considered that release from sequestration can serve to activate a variety of proteins. We then conceived of a system in which signaling-dependent proteolysis effectively integrates signaling over time, with output taking the form of a protein released from sequestration (Fig. 1B). We named this approach Rewiring of Aberrant Signaling to Effector Release (RASER).

We chose to develop the RASER concept first for oncogenic signaling by ErbB. Overexpression or mutation of ErbB receptors causes their constitutive phosphorylation at cytoplasmic tyrosine residues (3), which then bind to phosphotyrosine-binding (PTB) and SH2 domains (11). We first considered a simple system comprised of two components: a protease fused to PTB or SH2, and a cargo domain fused to a substrate sequence and a plasma membrane tether. In ErbB-hyperactive cells, protease recruitment to the membrane should allow it to cleave the substrate sequence and release cargo (Fig. 1B). We generated a simple mathematical model that predicts baseline cleavage rates of membrane-tethered vs. cytosolic substrates by proteases localized to the cytosol (supplementary text and fig. S1B,C). The model confirmed that membrane tethering of the substrate protein is sufficient to suppress cleavage by cytosolic protease in the baseline state, as desired (fig. S1C).

We used this simple model to select a sequence-specific protease from variants of hepatitis C virus (HCV) nonstructural protein 3 (NS3) protease or tobacco etch virus (TEV) protease. We chose the HCV NS3 protease without NS4A cofactor, as the model predicted it to release less cargo than TEV protease at baseline (fig. S1C), and as clinically approved small-molecule inhibitors of HCV protease are available for shutting off output if necessary. We selected the Shc PTB domain for fusion to the protease because its higher affinity for phospho-ErbB (pErbB) compared to SH2 domains (11) should maximize membrane localization. We designated the fusion of PTB and NS3 protease domain as PTB-pro. Finally, we designed a substrate fusion protein composed of the OFP orange fluorescent protein (OFP) as a test cargo fused to an HCV protease site and a CAAX membrane-localization signal, designated OFP-substrate-CAAX. We named this prototype system composed of PTB-pro and OFP-substrate-CAAX as ErbB-RASER0.1.

Building and testing a mathematical model of RASER

To enable rational optimization of RASER systems, we created a dynamic model of ErbB-RASER0.1 that predicts cargo accumulation over time in ErbB-off and ErbB-on states. The model required 11 parameters (fig. S1D) – production and degradation rate constants for protease and substrate components and for substrate fragments after cleavage, pErbB abundance (12–15), the k_{on} and k_{off} of the PTB-pErbB interaction (11), K_M and k_{cat} of the NS3-substrate reaction (16, 17), and the juxtamembrane volume in which ErbB cytosolic domains reside (fig. S1B). While we could obtain or estimate some parameters from published reports (fig. S1E and F), we calculated juxtamembrane volume from a molecular model (Fig. 1C), and measured component synthesis and degradation rates using our

previously described Small Molecule–Assisted Shutoff (SMASh) tag (18). SMASh tags shut off protein production upon drug addition and permit protein production when drug is removed, enabling measurement of protein decay or accumulation by immunoblotting (supplementary text and fig. S2). We then used the Haldane-Briggs implementation of Michaelis-Menten kinetics to calculate substrate cleavage rates from concentrations of protease and substrate, accounting for concentration of protease at the membrane and basal cleavage by unbound protease. The model predicted that cargo release should be enhanced in BT-474 cells, which express constitutively active ErbB2 (fig. S1F), compared to cells without ErbB2 activity. The degree of enhancement depended on protease speed (medium-cleaving NS3 or slow-cleaving NS3 with 54A mutation) and substrate affinity (high-affinity EDVVCC or medium-affinity DEMEEC), but in all cases was modest (Fig. 1D and E).

To test these predictions, we constructed and tested ErbB-RASER0.1. We tested both PTB-pro and PTB-pro(54A) protease components and OFP-EDVVCC-CAAX and OFP-DEMEEC-CAAX substrate components in BT-474 breast cancer cells that naturally overexpress ErbB2. Protease and substrate components were coexpressed from one transcriptional unit via a P2A ribosomal skipping sequence. For a matched ErbB-inactive control, we treated the same cells with the ErbB kinase inhibitor, lapatinib. By immunoblotting, we found that differences in product accumulation between ErbB-on and ErbB-off states closely matched those predicted by the model for PTB-pro (Fig. 1F and G), suggesting the usefulness of the model. However, cleavage rates for PTB-pro(54A) were lower in the experiment than in the model. This discrepancy may be a due to inaccuracy of the inputted K_M or k_{cat} values for pro(54A), which is NS3 protease with a 54A mutation and without the NS4A cofactor. Those values were estimated by combining the known individual effects of 54A mutation (16, 17) and NS4A loss (16, 17), but they may be inaccurate if the effects of these changes are not additive.

By confirming the model prediction of high basal cleavage with medium-speed protease and high-affinity substrate, these results also allowed us to further rule out the use of TEV protease, which exhibits even faster cleavage of its substrate. These results also confirmed that effector release was only weakly dependent on ErbB hyperactivity in ErbB-RASER0.1, indicating that further enhancement of ErbB-dependent release was needed.

Enhancing ErbB dependence of RASER by dual targeting

To improve RASER responses, we explored the possibility of co-recruiting the protease and substrate simultaneously to active ErbB receptors (Fig. 2A), which should increase the rate of protease-substrate encounters in the ErbB-on state. We first used structural modeling to find known phosphotyrosine sites on ErbB1 that can bring SH2-substrate fusions close enough to PTB-pro for cleavage without crowding, identifying pTyr-1016 as a suitable site (Fig. 2B). Next, we used the mathematical model, modified to include co-recruitment of protease and substrate to the receptor and possible rebinding of cleaved substrate, to predict how a range of SH2-ErbB affinities would affect accumulation of released cargo. Surprisingly, the model indicated that released cargo amounts were essentially invariant across all physiological SH2-ErbB affinities (11) (fig. S3A and B). We then constructed a series of substrate fusion proteins with SH2 domains that bind pTyr-1016, and assessed

cargo release upon cotransfection of PTB-pro and ErbB (fig. S4A). The VAV1 SH2 domain showed the largest enhancement in cargo release without toxicity (fig. S4B and C), and so was incorporated into the RASER system for testing *in silico* and *in cellulo*.

The model predicted that the dually targeted system composed of PTB-pro and OFP-DEMEEC-SH2-CAAX, designated ErbB-RASER0.2, should exhibit higher levels of OFP release compared to ErbB-RASER0.1 (Fig. 2C). Interestingly, the model also predicted lower cargo release without ErbB activity (Fig. 2C), because the measured half-life of OFP-DEMEEC-SH2-CAAX was shorter than that of OFP-DEMEEC-CAAX (fig. S4D). Indeed, testing of ErbB-RASER0.2 in BT-474 cells found actual cargo accumulation levels closely matching predicted levels (Fig. 2D and E). However, this system still cleaved a large amount (~30%) of substrate protein even in the absence of ErbB activity.

Enhancing ErbB dependence of RASER by selective protein destabilization

To enhance the ErbB dependence of RASER output, we next used the model to determine how to suppress cargo release selectively in the ErbB-off state. The model predicted that using the slower PTB-pro(54A) in place of PTB-pro would lead to lower substrate cleavage preferentially in the ErbB-off state (fig. S5A). However, we found that it also resulted in less cleavage in the ErbB-on state (fig. S5B). This discrepancy may again be due to the use of inaccurate K_M or k_{cat} values for pro(54A) in the model.

We thus considered other ways to reduce basal protease activity. Reducing protease production or increasing protease degradation would reduce basal cleavage and thereby enhance ErbB dependence (fig. S5C and D). However, rather than limiting protease abundance constitutively, we hypothesized that making protease stability itself dependent on ErbB activity could enhance the ErbB dependence of RASER output even further. We conceived of inserting a degron into the protease fusion protein so that its function would be inhibited by receptor binding (Fig. 2F), allowing the protease to accumulate to higher levels in cells with constitutively active ErbB. Specifically, we inserted into PTB-pro a short peptide degron from HIF1α at a loop of the PTB domain near the phosphopeptide binding groove, generating PTBHIF-pro (Fig. 2G). We confirmed ErbB-dependent stability of PTBHIF-pro but not PTB-pro using SMASh (Fig. 2H and fig. S6). We then tested a RASER system with PTBHIF-pro in place of PTB-pro *in silico* and *in cellulo*. The model predicted decreased cargo release in ErbB-off conditions (Fig. 2I), which was confirmed by experimentation in BT-474 cells (Fig. 2J and K). We named this optimized system ErbB-RASER1N, where N refers to the location of the cargo at the N-terminus of the substrate fusion protein.

Generalizability, selectivity, and robustness of RASER

One of the desirable features of the RASER design is its potential versatility in outputs, as various functional cargos can be incorporated into the substrate fusion protein. To further enhance versatility, we constructed a RASER variant to release cargo proteins from the C-terminus of the substrate protein. We tested a substrate protein composed of a signal peptide, the neurexin transmembrane segment (19), the VAV1 SH2 domain, an HCV protease

cleavage site, and the OFP cargo domain, and found it to respond as well as the OFP-site-SH2-CAAX substrate fusion (fig. S7A to C). We named the RASER system using PTBHIF-pro and this substrate protein as ErbB-RASER1C.

We next tested if ErbB-RASER responds to both ErbB1 and ErbB2 signaling and to different tumor types. The above experiments in BT-474 cells established responsiveness to ErbB2, so we first tested whether ErbB-RASER also responds to ErbB1 hyperactivity. We confirmed both ErbB-RASER1N and ErbB-RASER1C released cargo in response to coexpression of EGFRvIII, a constitutively active ErbB1 mutant, in MCF-7 cells, which otherwise exhibit normal levels of ErbB activity (fig. S7D). Next, we tested ErbB-RASER1N in various tumor cells that are hyperactive for ErbB signaling: BT-474 (ErbB2-overexpressing breast cancer), SK-BR3 (ErbB2-overexpressing breast cancer), SK-OV-3 (ErbB2-overexpressing ovarian cancer), H1975 (point-mutated ErbB1-expressing lung cancer), and LN-229:EGFRvIII (domain-deleted ErbB1-expressing glioma, (20)). Cargo was released in all cancer lines in an ErbB activity-dependent manner, with BT-474 cells producing cleaved cargo to a level 23-fold higher than ErbB-normal MCF-7 breast cancer cells (Fig. 3A,B). These results demonstrate that ErbB-RASER1N detects ErbB hyperactivity across many types of ErbB-positive cancer cells.

ErbB-RASER was designed to respond selectively to constitutive ErbB activity in cancer cells and not to transient ErbB activation that would occur in normal cells in response to EGF. We tested if this was indeed the case by comparing ErbB-normal cells in saturating EGF concentrations to ErbB-hyperactive cancer cells in basal EGF concentrations. In ErbB-normal MCF-7 cells, treatment with 50 nM EGF, a saturating concentration (21), for various times from 0.5 to 32 h did not induce cargo release from ErbB-RASER1N (Fig. 3C, fig. S8A). EGF treatment did upregulate phosphorylation of Akt and Erk, confirming that normal ErbB signaling was intact in these cells (Fig. 3C, fig. S8A). In contrast, cargo release was high in SK-BR-3 and BT-474 cells in media with 20 pM EGF, the basal concentration found in human blood (22) (Fig. 3C). The large difference in signal is not surprising, as SK-BR-3 and BT-474 overexpress ErbB. In addition, ErbB-normal cells respond to EGF for only 15 minutes (23) before strongly downregulating ErbB for hours afterwards (23, 24), whereas ErbB-hyperactive cancer cells either overexpress ErbB, causing saturation of degradation pathways, or express ErbB mutants that fail to be degraded (25). Regardless, as desired, ErbB-RASER1N selectively responds to constitutive ErbB activity but not to ligand-induced ErbB activation.

Finally, we asked whether ErbB-RASER is as responsive to oncogenic ErbB signaling as natural growth-promoting pathways. Interestingly, in BT-474 cells, ErbB-RASER1N output was more dependent on ErbB activity than endogenous Akt and Erk phosphorylation, with a response ratio of 36 compared to < 20 (Fig. 3D, top). Similar results were obtained in SK-OV-3, SK-BR-3, and LN-229:EGFRvIII cells as well (Fig. 3D, bottom and fig. S8B). Intriguingly, in SK-OV-3 cells, expression of the RASER system clearly inhibited endogenous Erk phosphorylation (Fig. 3D, bottom). This inhibitory effect can be explained by RASER components competing with endogenous signaling molecules for binding to phosphorylated ErbB, resulting in rewiring of signaling from Erk activation to cargo release.

Rewiring ErbB hyperactivity to apoptosis with RASER

We next programmed ErbB-RASER to produce therapeutically useful outputs. We envisioned that, following delivery of ErbB-RASER *in vivo*, these outputs would be activated in ErbB-dependent cancer cells but not in normal cells. One potentially useful output could be cell killing. We found that OFP fused to the BH3 domain of Bid (referred to as OFP-Bid) or Bax to be potent apoptosis inducers (fig. S9A). We thus used OFP-Bid as cargo to rewire oncogenic ErbB signaling to apoptosis (Fig. 4A). We created a single transcriptional unit co-expressing both substrate and protease components of ErbB-RASER to release OFP-Bid, named ErbB-RASER1C-Bid (Fig. 4B). Indeed, we found that in ErbB2-overexpressing BT-474 breast cancer cells, transfection of ErbB-RASER1C-Bid induced PARP cleavage, a marker of apoptosis, to 99% of the levels induced by Bid alone (Fig. 4C,D). This effect was dependent on ErbB activity, as it was blocked by lapatinib (fig. S9B). If RASER were to be clinically useful, then ErbB-RASER1C-Bid should not kill cells without hyperactive ErbB. Indeed, expression of ErbB-RASER1C-Bid induced apoptosis in ErbB-normal MCF-7 cells with only 5% efficiency compared to Bid alone (Fig. 4C,D). To further establish the generalizability of RASER to different apoptosis-inducing cargoes, we also constructed ErbB-RASER1N-Bax, in which ErbB activity is linked to release of Bax as cargo (fig. S10A). Expression of ErbB-RASER1N-Bax also induced apoptosis in ErbB2-overexpressing BT-474 cells, but not in ErbB-normal MCF-7 cells (fig. S10B and C).

As RASER would need to be delivered by viruses for *in vivo* applications, we also tested RASER performance under viral expression conditions. Lentiviral transduction of ErbB-RASER1C-Bid efficiently induced apoptosis in BT-474 cells but not MCF-7 cells, as visualized by a caspase-activated fluorescent dye (Fig. 4E). Indeed, apoptosis occurred in nearly all transduced BT-474 cells, but no transduced MCF-7 cells. ErbB-RASER1C-Bid also caused apoptosis in the ErbB1-dependent lines H1975 and LN-229:EGFRvIII (Fig. 4F–H, fig. S10D). These results demonstrate that RASER can be programmed to directly induce apoptosis in response to constitutive ErbB activity, and that virally delivered RASER can selectively kill ErbB-driven cancer cells.

Rewiring ErbB hyperactivity to transcription of endogenous genes with RASER

A particularly powerful and versatile set of RASER outputs would be the transcription of specific endogenous genes, as a variety of cellular phenotypes or functions could be induced by activating endogenous genes. We thus explored using transcriptional activators as RASER cargoes. First, we verified that the synthetic transcription factor tTA could be released from ErbB-RASER1N-tTA and activate transcription in an ErbB-dependent manner (fig. S11A–D). Next, to test that RASER could mediate activation of endogenous genes to induce a biological response, we used constitutively active FoxO3 (caFoxO3), which activates pro-apoptotic genes (26), as cargo (fig. S11E). ErbB-RASER1N-caFoxO3 expression in ErbB-hyperactive BT-474 cells induced apoptosis with comparable efficiency as caFoxO3 alone (fig. S11F,G). Thus, RASER can indeed be used to rewire ErbB hyperactivity to the activation of either transgenes or endogenous genes.

To rewire ErbB hyperactivity to the regulation of essentially any endogenous gene, we explored the use of CRISPR/Cas9 domains as RASER cargoes. We constructed RASER systems for ErbB-dependent release of catalytically dead Cas9 fused to transcriptional activation domains (Cas9VP64 or VPRdCas9) (27, 28), and coexpressed them with guide RNAs (gRNAs) to target genes of interest (Fig. 5A, fig. S12A). In initial tests with gRNAs directed to a cotransfected reporter, we observed that both dCas9VP64- and VPRdCas9-based systems activated transcription specifically in ErbB hyperactive cells, as desired (Fig. 5B,C and fig. S14B and C).

We then asked whether we could use ErbB-RASER1C-dCas9VP64 to link ErbB hyperactivity to the transcription of endogenous genes. An endogenous gene whose activation in a cancer cell could be therapeutically useful is *CSF2*, encoding GM-CSF. GM-CSF induces antigen-presenting dendritic cells to present antigens released from tumor cells, in turn activating cytotoxic T lymphocytes recognizing those antigens (29). However, in clinical trials, systemic GM-CSF injections have shown limited anti-tumor efficacy while causing toxicity from off-target immune reactions (30). Inducing GM-CSF expression specifically in tumor cells *in situ* may elicit more effective immune responses than systemic GM-CSF and indeed is an essential mechanism of action for an oncolytic virus recently approved for clinical use (31).

To enable targeted activation of *CSF2* transcription in ErbB-driven cancer cells by RASER (Fig. 5D), we identified a gRNA that could mediate effective transcriptional activation of *CSF2* (fig. S12D). We then introduced the combination of ErbB-RASERC1-dCas9VP64, SAM transactivation components (27), and the optimal gRNA into cells with either ErbB hyperactivity or normal ErbB activity, and assayed for GM-CSF protein in the cell media. We found that GM-CSF production was efficiently upregulated in cells with hyperactive ErbB, reaching 87% of that of an untethered dCas9VP64 control, but remained low in cells with normal ErbB activity (Fig. 5E,F). These results demonstrate that RASER can indeed rewire oncogenic ErbB signaling to activation of endogenous genes of choice using dCas9 proteins.

Efficacy and specificity of the RASER-induced apoptosis

To explore the potential utility of RASER for cancer treatment, we compared it to standards of care for efficacy and specificity in killing cancer cells. Two ErbB-hyperactive cancer lines (BT-474 breast cancer and H1975 lung cancer), an ErbB-negative cancer line (MCF-7 breast cancer), and two non-cancerous cell lines (MCF-10A breast epithelium and MRC5 lung fibroblast) were each treated with carboplatin and paclitaxel combination chemotherapy, targeted ErbB inhibitor lapatinib, or a lentivirus expressing ErbB-RASER1C-Bid. The first two treatments are first-line standards of care for metastatic breast and lung cancer, with lapatinib reserved for ErbB-positive cases (32–35). We found that carboplatin and paclitaxel killed cells non-selectively, regardless of tumorigenicity or ErbB status (Fig. 6A). Lapatinib cytotoxicity varied by cell line, but did not consistently correlate with ErbB status (Fig. 6A). In contrast, lentivirus-mediated transduction of ErbB-RASER1C-Bid induced high rates of cell death in the two ErbB-hyperactive tumor cell lines while having negligible effects on any of the ErbB-normal cells, as desired (Fig. 6A). Imaging experiments confirmed that

RASER exhibited superior selectivity and higher cytotoxicity in ErbB-hyperactive cancer cells than paclitaxel (Fig. 6B). Thus, RASER demonstrated greater specificity and efficacy compared to current clinical treatments for ErbB-positive cancers.

To further demonstrate its therapeutic potential, we tested RASER in a co-culture model of disseminated cancer with delivery by recombinant adeno-associated virus (rAAV). To model liver dissemination of pancreatic cancer, which carries a poor prognosis and for which surgical resection is not possible (36), we differentiated human Huh7.5-GFP cells, which express normal levels of ErbB, into hepatocyte-like cells (37), then overlaid either ErbB1-hyperactive human BxPC3 pancreatic cancer cells (38) or, for comparison, ErbB-normal MCF-7 cancer cells. To maximize translational potential, we used rAAV to deliver ErbB-RASER1C-Bid (fig. S13A), as rAAV is the only viral vector currently approved for gene delivery to normal tissues in the body, due to its lack of pathogenicity and genotoxicity (39). mCardinal-expressing control rAAVs alone were not toxic to either BxPC3 or MCF-7 cells (fig. S13B), and ErbB-RASER-Bid-expressing and control mCardinal-expressing rAAVs were similarly infectious (fig. S13B,C). As expected, while rAAV-ErbB-RASER1C-Bid had no effect on MCF-7 cells, with the OFP-Bid cargo retained at the cell membrane (fig. S13C), rAAV-ErbB-RASER1C-Bid released OFP-Bid and induced apoptosis in BxPC3 cells (fig. S13C, S14A).

Finally, we treated the Huh7.5-BxPC3 cocultures with rAAV-ErbB-RASER1C-Bid or control rAAV (Fig. 6C). As desired, rAAV-ErbB-RASER1C-Bid selectively killed the ErbB-hyperactive BxPC3 cells while sparing the cocultured Huh7.5 hepatocytes (Fig. 6D,E and fig. S14C). In contrast, when the ErbB-normal MCF-7 cells were cocultured with Huh7.5 hepatocytes, rAAV-ErbB-RASER1C-Bid killed neither cell type (Fig. 6D,E), confirming the specificity of ErbB-RASER1C-Bid output for ErbB-hyperactive cells. Thus, ErbB-RASER-Bid delivered by rAAV selectively ablates ErbB-positive pancreatic cancer cells in a co-culture model of disseminated cancer, demonstrating that RASER indeed exhibits highly selective anti-cancer activity.

Discussion

In summary, we used protein engineering and computational modeling to develop a molecular signal integrator called RASER that specifically detects oncogenic signaling and rewires it to a variety of functional outputs. Interestingly, RASER responds selectively to constitutive oncogenic ErbB signaling and not to normal ligand-induced signaling, and is more responsive to oncogenic ErbB than natural growth-promoting pathways. We demonstrated the ability of RASER to kill or induce endogenous gene transcription specifically in ErbB-driven cancer cells. Notably, we obtained all our results in populations of heterogeneously transfected or transduced cells, without sorting, selection, or cloning for uniform expression, demonstrating the robustness of RASER.

As a synthetic signaling pathway, RASER has several unique attributes. It is both compact and highly responsive, which derives from the use of a protease to simultaneously sense and transduce a signal. This enables high levels of amplification without requiring signaling cascades or transcriptional steps. The compactness and modularity of RASER also allows its

behavior to be accurately simulated by a mathematical model, which aids in system optimization. Finally, the use of modular domains for cancer sensing suggests that RASER systems can be engineered to detect various types of cancers or execute various therapeutic programs.

Besides its programmability, RASER may have other advantages over conventional therapies. First, because RASER selectively targets constitutively active signals found only in cancer cells, it may be less toxic than treatments targeting biochemical processes or antigens present in both cancer and normal cells. Second, the development of resistance to RASER may be difficult. Resistance to small-molecule inhibitors can arise from mutations that disrupt target binding or increase target expression (40), while resistance to monoclonal antibodies or chimeric antigen receptor (CAR)-expressing T cells can occur from decreased antigen expression, mutations in the epitope sequence, or alternative splicing around the epitope (41, 42). In contrast, RASER is activated by the same signals that tumor cells rely on for proliferation and survival. Thus cancer cells harboring resistance mutations that preserve or further elevate ErbB function will continue to activate RASER. For instance, non-small cell lung cancers (NSCLCs) treated with first-generation ErbB inhibitors such as lapatinib inevitably acquire resistance, with > 50% of cases resulting from a T790M mutation in ErbB1 (43). However, as would be expected from its design, we found that ErbB-RASER was activated in H1975 cells, a NSCLC line expressing T790M-mutant ErbB1.

Over the last two decades, the most common strategy for restricting the effects of genetically encoded therapy to cancer cells has been the use of promoters that demonstrate higher activity in cancer cells than normal cells (44, 45). However, cancer-selective promoters are weak compared to constitutive promoters, and often lose cancer specificity in the context of non-integrating viruses (44, 46). Multi-gene circuits can be designed to enhance specificity and amplify signal (45), but require the integration of multiple transgenes into the genome. As this creates risks of insertional mutagenesis, the clinical applicability of such multi-gene circuits remains unclear. In contrast, RASER does not depend on transcriptional mechanisms for cancer detection and is compact enough to be expressed from non-integrating viruses with proven safety profiles, such as adeno-associated virus.

In using a proteolytic event to trigger effector release, RASER is reminiscent of several recently developed chimeric receptors such as synNotch (47), TANGO (48), and MESA (49). However, these receptors are distinct from RASER in that they, like natural transmembrane receptors, respond to stimuli outside the cell. These receptors may find use in customizing the responses of immune cells to tumor antigens, in effect generalizing the concept of CARs to different intracellular outputs (7–9). In contrast, RASER specifically senses oncogenic signals within tumor cells and rewires them to therapeutic responses.

An intriguing possible implementation of RASER may be to generate pathway-specific oncolytic viruses, taking advantage of the ability of viruses to penetrate solid tumors more effectively than cell-based therapies (50). We demonstrated that ErbB-RASER-Bid delivery by nonpathogenic viral vector rAAV can specifically kill ErbB-positive cancer cells and spare normal cells. As rAAV does not naturally have tumor-selective tropism or lytic ability, these results can be viewed as converting the non-pathogenic rAAV into to a tumor-selective

cytotoxic virus by expressing ErbB-RASER-Bid. We also demonstrated the ability of RASER to induce cytokine release. Interestingly, systemic anti-tumor effects can be elicited by cytokine release from a subset of tumor cells (45), so RASER may not need to be delivered to every tumor cell in therapeutic applications if programmed to induce immunostimulation. In such a context, RASER may benefit from combination with current immunotherapies. However, while RASER viruses may function well against cancer cells in culture, additional modifications may be required for them to be efficacious and non-toxic *in vivo*. Some well known challenges common to virotherapy that need to be overcome, for example, include producing sufficient viral titers, obtaining high-efficiency infections of tumors, and avoiding premature immune clearance. Solving these issues may benefit from systematic testing in immunocompetent animal cancer models of multiple parameters including viral vector types, administration routes and doses, methods to target viruses to specific cell-surface receptors, and treatments to suppress humoral immunity.

In conclusion, as a molecular integrator tuned for specifically detecting oncogenic signals, RASER represents a novel type of synthetic biological device. RASER robustly links oncogenic signals to a wide array of programmable outputs, and its design provides a template for future computer-assisted engineering of other synthetic signaling pathways. Most importantly, RASER introduces the possibility of signal rewiring as a new approach to cancer treatment.

Supplementary Material

Refer to Web version on PubMed Central for supplementary material.

Acknowledgements:

We thank M. Covert (Stanford University) for advice on mathematical modeling, and members of the Lin laboratory for advice and assistance with experiments. We also thank J. S. Glenn (Stanford University), H. Chang (Stanford University), R. Levy (Stanford University), H. Dai (Stanford University), S. Gambhir (Stanford University), and X. Shu (UCSF) for cell lines, and S.W. Cho of the Chang laboratory for training on qRT-PCR.

Funding: This work was supported by a Stanford Graduate Fellowship and an Ilju Foundation Predoctoral Scholarship (H.K.C.), NIH/NIGMS EUREKA grant 5R01GM098734 (M.Z.L.), a Burroughs Wellcome Foundation Career Award for Medical Scientists (M.Z.L.), a Damon Runyon-Rachleff Innovation award (M.Z.L.), an Alliance for Cancer Gene Therapy Young Investigator Award (M.Z.L.), and NIH/NIGMS center grant P50GM107615 (J.E.F., M.Z.L.).

References and Notes:

1. Ye H, Fussenegger M, FEBS Lett 588, 2537 (2014). [PubMed: 24844435]
2. Torti D, Trusolino L, EMBO Mol Med 3, 623 (2011). [PubMed: 21953712]
3. Mishra R, Hanker AB, Garrett JT, Oncotarget 8, 114371 (2017). [PubMed: 29371993]
4. Zhang H et al., J Clin Invest 117, 2051 (2007). [PubMed: 17671639]
5. Miest TS, Cattaneo R, Nat Rev Microbiol 12, 23 (2014). [PubMed: 24292552]
6. Whilding LM, Maher J, Immunotherapy 7, 229 (2015). [PubMed: 25804476]
7. Higashikuni Y, Chen WC, Lu TK, Curr Opin Biotechnol 47, 133 (2017). [PubMed: 28750201]
8. Ho P, Chen YY, Curr Opin Chem Biol 40, 57 (2017). [PubMed: 28628856]
9. Lienert F, Lohmueller JJ, Garg A, Silver PA, Nat Rev Mol Cell Biol 15, 95 (2014). [PubMed: 24434884]
10. Hynes NE, Lane HA, Nat Rev Cancer 5, 341 (2005). [PubMed: 15864276]

11. Jones RB, Gordus A, Krall JA, MacBeath G, Nature 439, 168 (2006). [PubMed: 16273093]
12. DeFazio-Eli L et al., Breast Cancer Res 13, R44 (2011). [PubMed: 21496232]
13. Friedrich K et al., Mol Ther 21, 849 (2013). [PubMed: 23380817]
14. Okabe T et al., Cancer Res 67, 2046 (2007). [PubMed: 17332333]
15. Zhang F et al., Anal Chem 87, 9960 (2015). [PubMed: 26368334]
16. Landro JA et al., Biochemistry 36, 9340 (1997). [PubMed: 9235976]
17. Tong X et al., Antiviral Res 70, 28 (2006). [PubMed: 16448708]
18. Chung HK et al., Nat Chem Biol 11, 713 (2015). [PubMed: 26214256]
19. Wang W et al., Nat Biotechnol 35, 864 (2017). [PubMed: 28650461]
20. Fan QW et al., Cancer Cell 24, 438 (2013). [PubMed: 24135280]
21. Kozer N et al., Phys Biol 8, 066002 (2011). [PubMed: 21946082]
22. Marquèze-Pouey B, Mailfert S, Rouger V, Goaillard JM, Marguet D, PLoS One 9, e106803 (2014). [PubMed: 25265278]
23. Zheng Y et al., Nature 499, 166 (2013). [PubMed: 23846654]
24. Carter RE, Sorkin A, J Biol Chem 273, 35000 (1998). [PubMed: 9857032]
25. Sigismund S, Avanzato D, Lanzetti L, Mol Oncol 12, 3 (2018). [PubMed: 29124875]
26. Brunet A et al., Cell 96, 857 (1999). [PubMed: 10102273]
27. Konermann S et al., Nature 517, 583 (2015). [PubMed: 25494202]
28. Chavez A et al., Nat Methods 12, 326 (2015). [PubMed: 25730490]
29. Hamilton JA, Nat Rev Immunol 8, 533 (2008). [PubMed: 18551128]
30. Arellano M, Lonial S, Biologics 2, 13 (2008). [PubMed: 19707424]
31. Kohlhapp FJ, Kaufman HL, Clin Cancer Res 22, 1048 (2016). [PubMed: 26719429]
32. Alsharedi M, Gress T, Dotson J, Elmsherghi N, Tirona MT, Med Oncol 33, 27 (2016). [PubMed: 26883934]
33. Boyd LR, Muggia FM, Oncology (Williston Park) 32, 418 (2018). [PubMed: 30153322]
34. Socinski MA, Curr Oncol 21, e691 (2014). [PubMed: 25302040]
35. Pimenta L, Dornelas M, Cezana L, N Engl J Med 374, 2602 (2016).
36. Yamada H, Hirano S, Tanaka E, Shichinohe T, Kondo S, HPB (Oxford) 8, 85 (2006). [PubMed: 18333251]
37. Choi S, Sainz B, Corcoran P, Uprichard S, Jeong H, Xenobiotica 39, 205 (2009). [PubMed: 19280519]
38. Walsh N et al., Invest New Drugs 31, 558 (2013). [PubMed: 23076814]
39. Naso MF, Tomkowicz B, Perry WL, Strohl WR, BioDrugs 31, 317 (2017). [PubMed: 28669112]
40. Paez JG et al., Science 304, 1497 (2004). [PubMed: 15118125]
41. Fry TJ et al., Nat Med 24, 20 (2018). [PubMed: 29155426]
42. Reslan L, Dalle S, Dumontet C, MAbs 1, 222 (2009). [PubMed: 20065642]
43. Skoulidis F, Papadimitrakopoulou VA, Clin Cancer Res 23, 618 (2017). [PubMed: 27821604]
44. Dorer DE, Nettelbeck DM, Adv Drug Deliv Rev 61, 554 (2009). [PubMed: 19394376]
45. Nissim L et al., Cell 171, 1138 (2017). [PubMed: 29056342]
46. Kanegae Y et al., Nucleic Acids Res 39, e7 (2011). [PubMed: 21051352]
47. Morsut L et al., Cell 164, 780 (2016). [PubMed: 26830878]
48. Barnea G et al., Proc Natl Acad Sci U S A 105, 64 (2008). [PubMed: 18165312]
49. Schwarz KA, Daringer NM, Dolberg TB, Leonard JN, Nat Chem Biol 13, 202 (2017). [PubMed: 27941759]
50. Fountzilas C, Patel S, Mahalingam D, Oncotarget 8, 102617 (2017). [PubMed: 29254276]

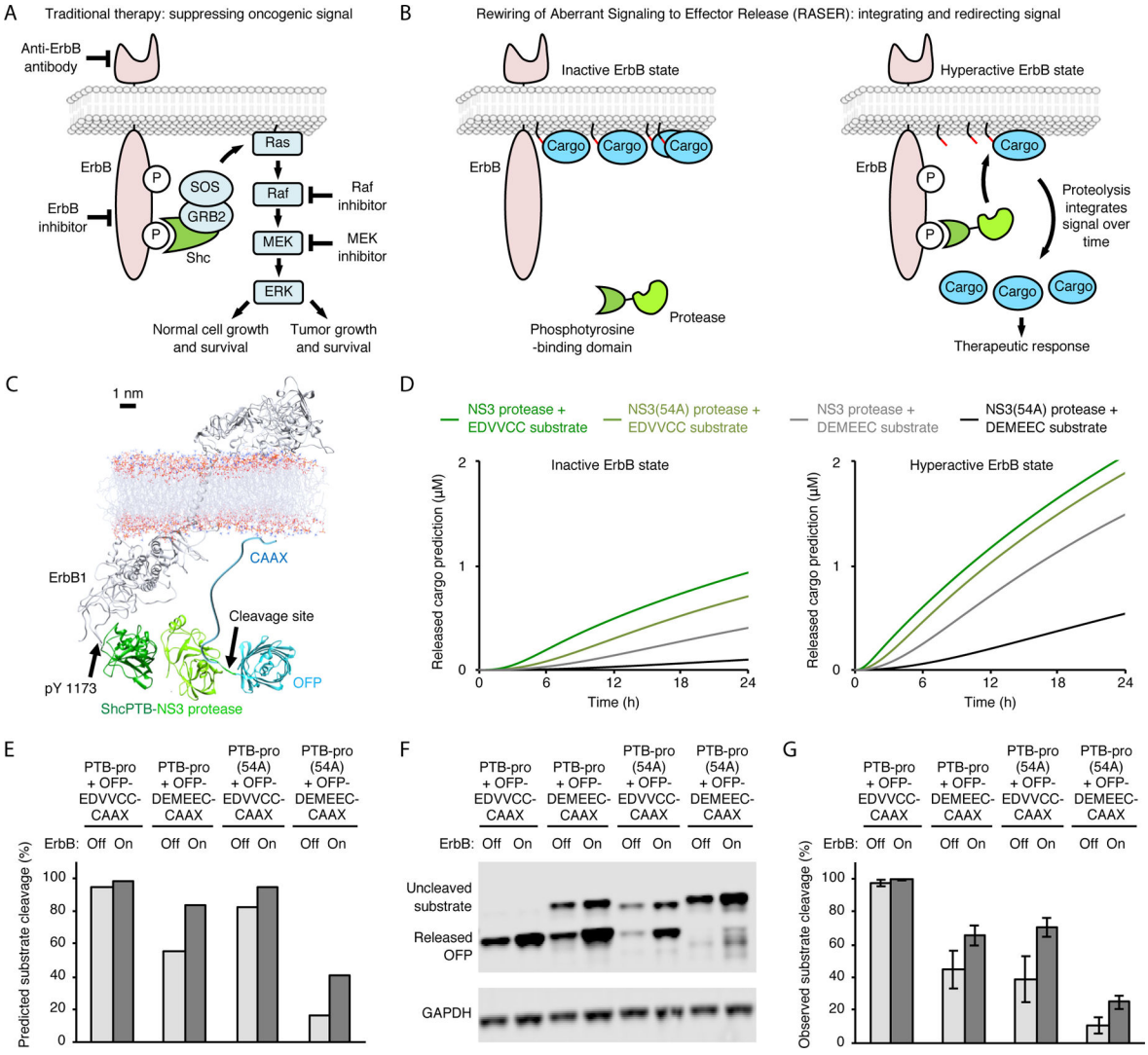

Fig. 1.

Concept and model of a molecular integrator of ErbB signaling. (**A**) Pharmacological approaches to cancer therapy that aim at blocking tumor-promoting signals. (**B**) Signal-induced proteolysis can integrate signal activity over time and function as a generalizable activation mechanism for multiple effectors. (**C**) Molecular modeling suggests the OFP-substrate-CAAX protein should be able to be cleaved by PTB-pro bound to ErbB. (**D**) Predicted concentration of released cargo at various times in ErbB-inhibited and ErbB-hyperactive states, using ErbB numbers from BT-474 breast cancer cells. (**E**) Predicted percent substrate cleavage after 24 h of protein expression. Note percent substrate cleavage is not the same as concentration of cleaved cargo, because the model accounts for the observation that ~50% less total substrate is expressed in ErbB-inhibited conditions. Predicted percent substrate cleavage normalizes for this expression difference whereas the predicted concentration of released cargo does not. (**F**) Observed cleavage efficiency by protease and substrate variants. BT-474 cells, in which ErbB2 (HER2) is overexpressed and constitutively active, were transfected with the indicated constructs. Cells were then

incubated with 0.5 μM lapatinib to inhibit ErbB or without lapatinib to leave ErbB signaling on. After 24 h, cells were lysed for immunobloting against the V5 epitope tag fused to OFP. GAPDH served as a loading control. (**G**) Observed percent substrate cleavage. Error bars represent standard error of the mean (s.e.m.) of three biological replicates.

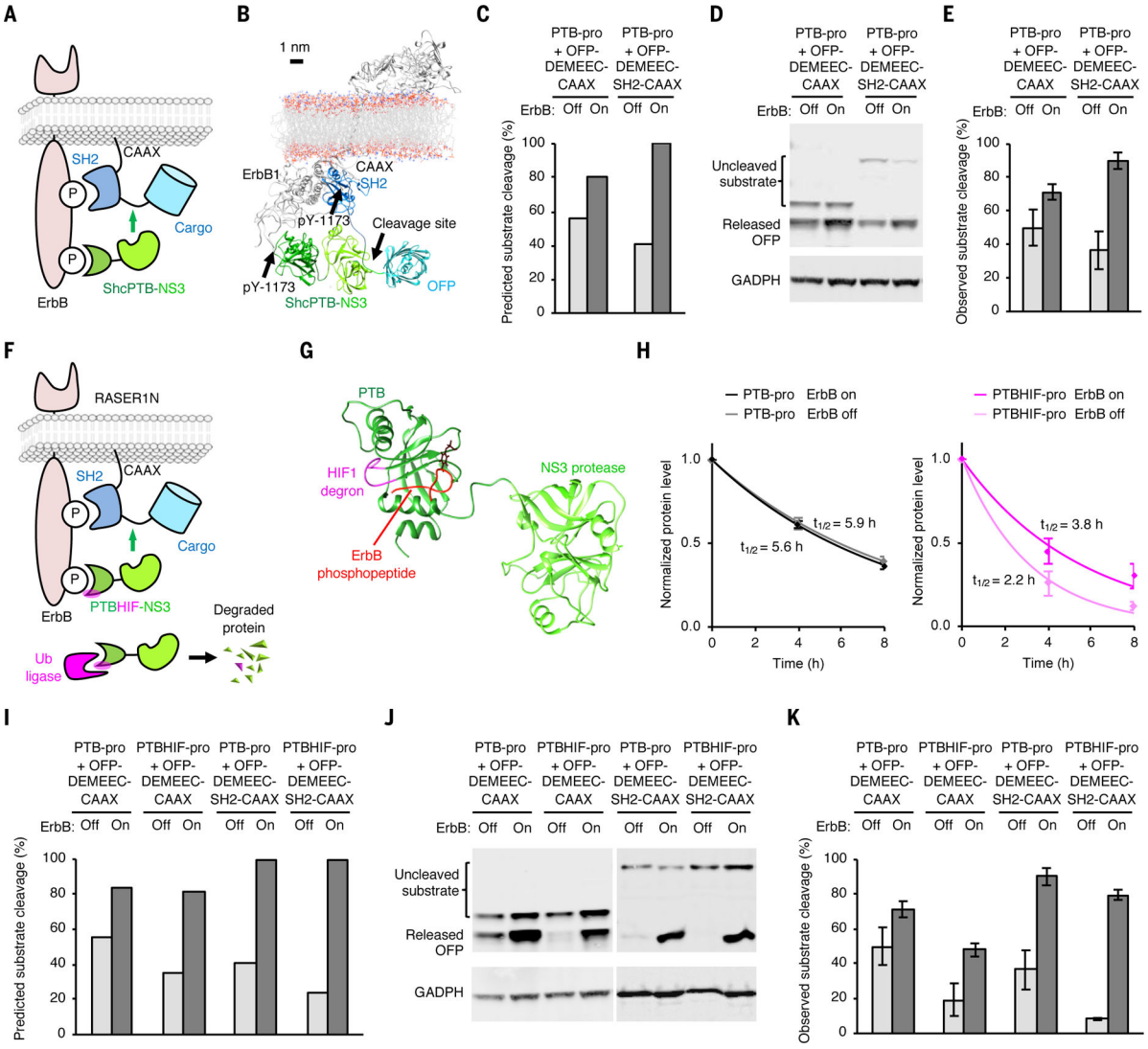

Fig. 2.

Development of the final ErbB-RASER system. (**A**) Schematic of the dual-targeted system. The substrate fusion is recruited to active receptor via an SH2 domain to facilitate cleavage at the substrate sequence (green line between SH2 and cargo). (**B**) Atomic model of the dual-targeted system. (**C**) Predicted substrate cleavage after 24 h of protein expression. (**D**) Observed cleavage by the mono- and dual-targeted systems. Experiments were performed as in Fig. 1. (**E**) Quantitation of observed substrate cleavage. Error bars represent s.e.m. of three biological replicates. (**F**) Schematic of the ErbB-RASER1N system, composed of a substrate fusion protein bearing a cargo domain at the N-terminus (cargo-DEMEEC-SH2-CAAX) and a fusion protein of a PTB domain with a HIF1α degron insert and a HCV NS3 protease domain (PTBHIF-pro). (**G**) Structural model of PTBHIF-pro. The HIF1α degron (magenta) is inserted in the loop near the phosphorylated peptide (red) binding site. (**H**) Half-life measurement of PTB-pro and PTBHIF-pro in ErbB-on and ErbB-off states in BT-474 cells. Background-subtracted protein signal was normalized to background-subtracted GAPDH signal and then divided by the mean signal at 0 h (n = 3, error bars

represent s.e.m.). Values fit an exponential decay to calculate half-lives. (**I**) Prediction of percent substrate cleavage at 24 h of protein expression. (**J**) ErbB-RASER1N releases OFP in a ErbB- and SH2-dependent manner in ErbB-hyperactive BT-474 cells. (**K**) Experimentally observed cleavage efficiency of RASER1N. Error bars represent s.e.m. of three biological replicates.

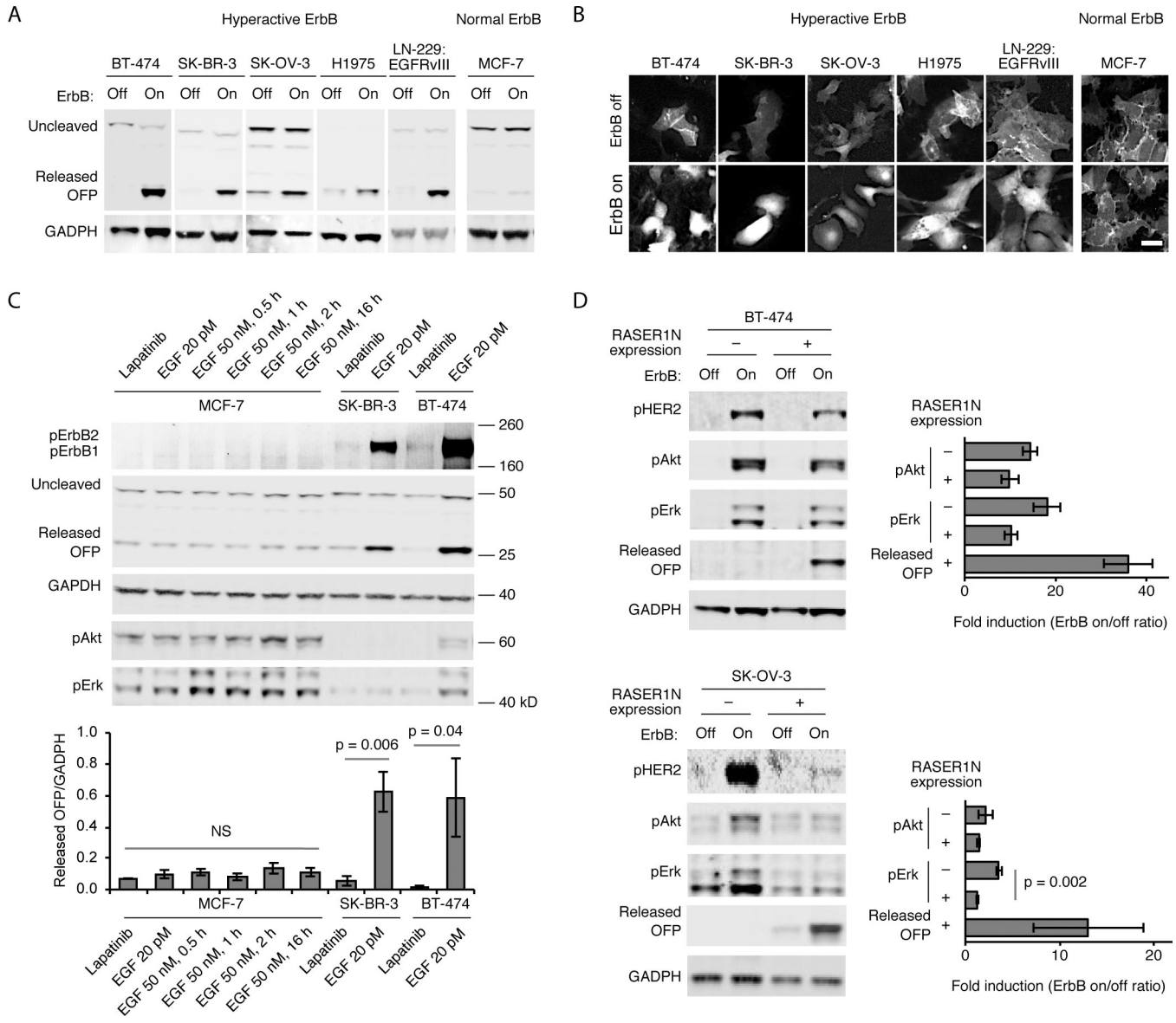

Fig. 3.

Generalizability, specificity, and responsivity of RASER to ErbB hyperactivity. (**A**) Generalization of RASER1N to ErbB-hyperactive cancer lines. OFP is released in ErbB-hyperactive cancer lines BT-474 and SK-BR-3 (breast cancer), SK-OV-3 (ovarian cancer), H1975 (lung cancer) and LN-299:EGFRvIII (glioblastoma) in an ErbB-dependent manner, as assessed by immunoblotting. In contrast, ErbB-normal MCF-7 cells did not show OFP release. All cells were cultured in media with 10% fetal bovine serum. The ErbB-off state was produced by incubation with 0.1 osimertinib for H-1975 cells, which are resistant to lapatinib, or 0.5 μM lapatinib for all other cells. The ErbB-on state represents the default state in 10% serum without additional EGF stimulation for all cell types in this panel. (**B**) Fluorescence microscopy of (A). Scale bar, 50 μm. (**C**) RASER1N is specific for constitutively active ErbB, rather than ErbB transiently activated by EGF stimulation. ErbB-normal MCF7 or ErbB-hyperactive SK-BR-3 and BT-474 cells were infected with lentivirus

expressing ErbB-RASER1N with OFP cargo in media supplemented with 10% serum and EGF at 20 pM, its baseline concentration in human blood. 48 h after transduction, MCF-7 cells were stimulated by 50 nM EGF, a saturating concentration, for 1–16 h. Top, After stimulation, cells were lysed for immunoblotting of pErbB, OFP, GAPDH, pAkt and pErk. Bottom, quantitation of OFP immunoblot signals normalized to GAPDH levels. Differences between conditions in MCF-7 cells were not significant (NS, $p = 0.47$ by single-factor ANOVA). Higher RASER outputs in the basal condition (20 pM EGF) compared to the lapatinib-inhibited state in SK-BR-3 and in BT-474 cells were statistically significant by two-tailed unpaired t test. (**D**) RASER output is comparable to endogenous pathways downstream of active ErbB. Cells were cultured in media with 10% serum. Left, activation of Akt, Erk, and RASER was assessed by immunoblotting in ErbB-dependent cancer cells with or without expression of ErbB-RASER1N with OFP cargo. Right, fold induction of Akt, ERK, and RASER activity. The difference in pErk between RASER-expressing and -nonexpressing cells was statistically significant by two-tailed unpaired t test. All error bars represent s.e.m. of three biological replicates.

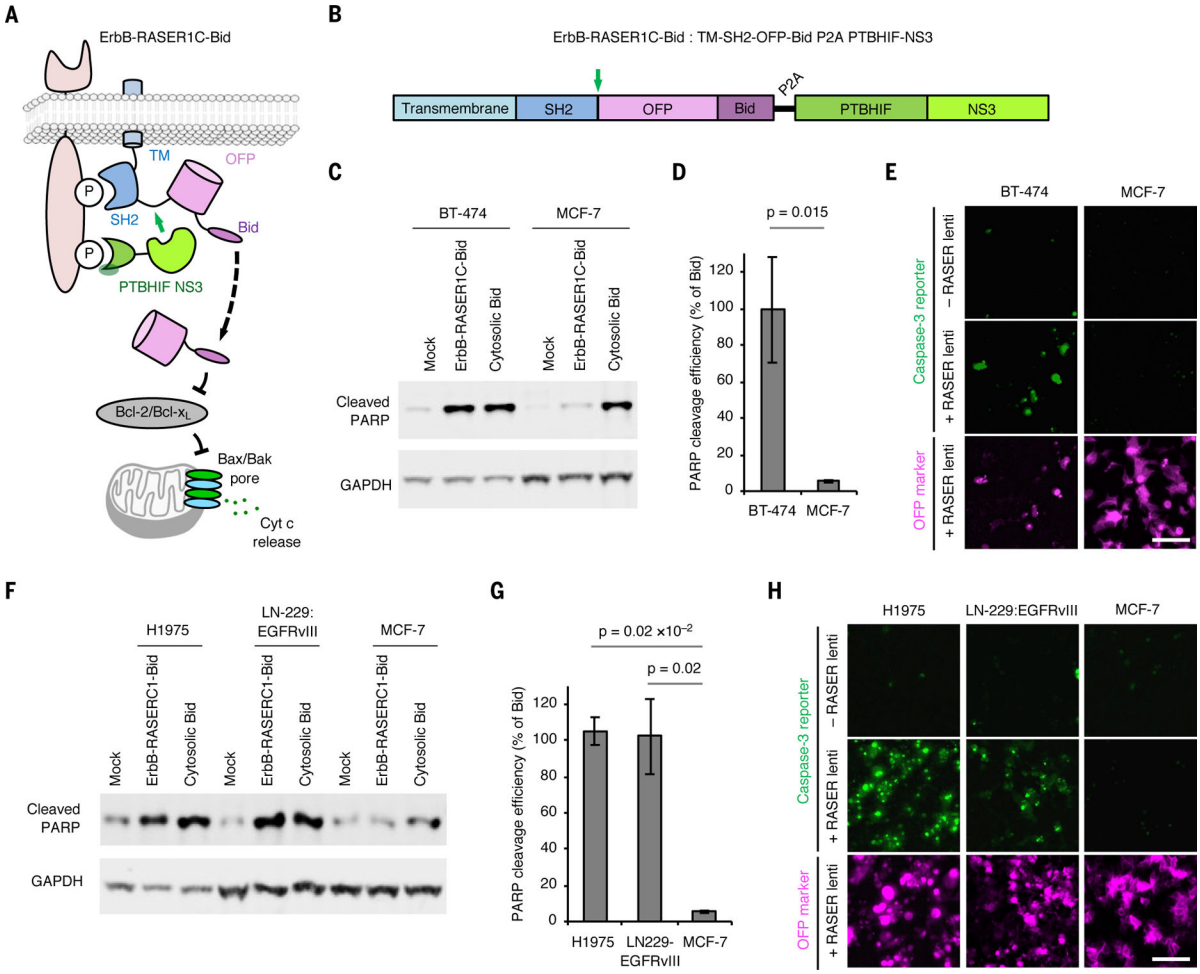

Fig. 4.

RASER can be programmed to induce apoptosis selectively in ErbB-driven cancer cells. (**A**) Schematic description of the ErbB-RASER1C-Bid system. OFP-Bid will be released in the presence of constitutive ErbB signaling. (**B**) ErbB-RASER1C-Bid is a single transcription unit encoding both substrate and protease components that can be expressed at a constant ratio by transfection with a single plasmid or transduction by a single virus. Green arrow, protease cleavage site to release cargo. (**C**) BT-474 cells which overexpress ErbB2 and MCF7 cells with normal ErbB levels were transfected with the ErbB-RASER1C-Bid construct. After 16 h of protein expression, cells were lysed for immunoblotting to detect cleaved PARP and GAPDH. (**D**) Quantitation of cleaved PARP levels in immunoblots. Error bars represent s.e.m. of three biological replicates. The increased RASER output in BT-474 cells compared to MCF-7 cells was statistically significant by one-tailed unpaired t test. (**E**) ErbB-RASER1C-Bid virus infection efficiently induced apoptosis in BT-474 cells but not MCF-7 cells. Apoptosis was visually assessed using a fluorescent caspase-3 activity indicator. Scale bar, 100 μm. (**F**) Apoptosis inductivity of ErbB-RASER1C-Bid is generalizable in multiple ErbB1 hyperactive cancer cell lines. H1975, LN-229:EGFRvIII and MCF-7 cells were tested in a same method to (B). (**G**) Quantification of cleaved PARP level, calculated as in (C). (**H**) Infection with virus expressing ErbB-RASER1C-Bid induced

apoptosis in H1975 and LN-229:EGFRvIII cells, which express hyperactive ErbB1 mutants, but not MCF-7 cells which does not express hyperactive ErbB. Apoptosis was visually assessed using a fluorescent caspase-3 activity indicator. Scale bar, 100 μm.

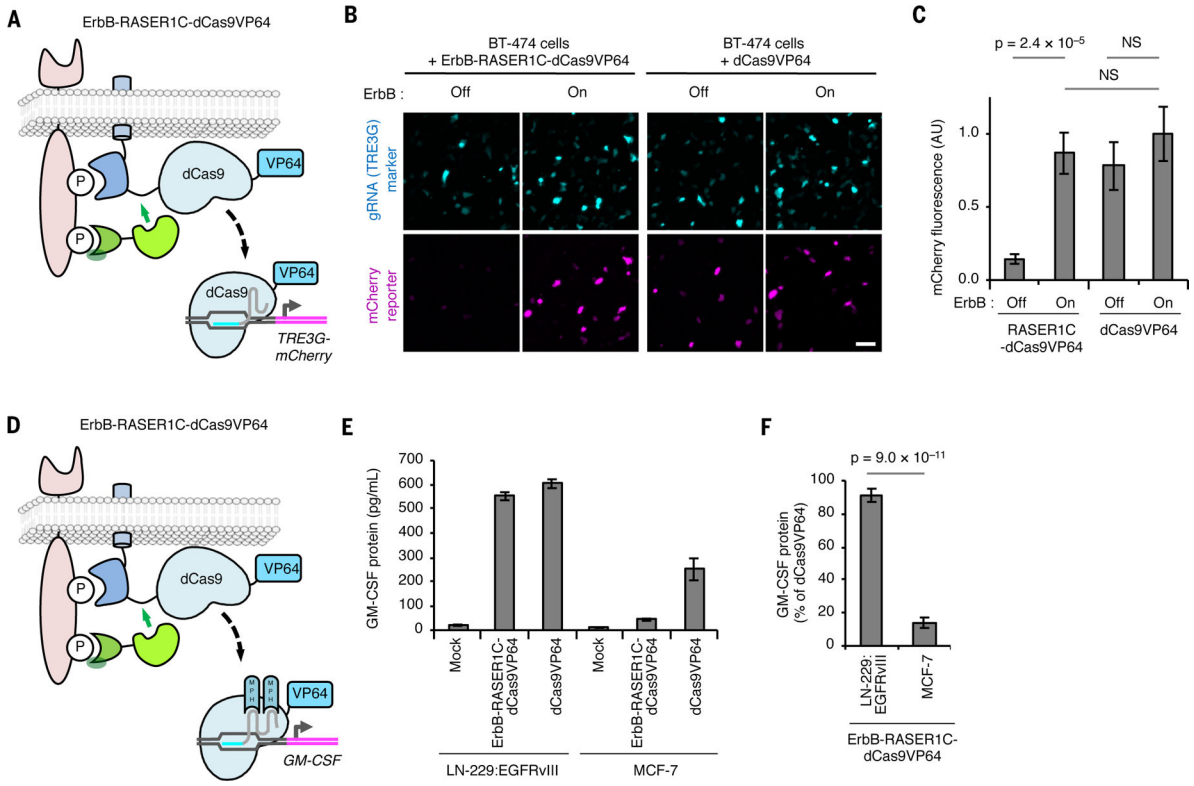

Fig. 5.

RASER can be programmed to activate endogenous genes of choice selectively in ErbB-driven cancer cells. (**A**) Schematic of the ErbB-RASER1C-dCas9VP64 system regulating a reporter gene. dCas9 with a VP64 transcriptional activation domain will be released in the presence of constitutively active ErbB to activate TRE3G-mCherry. (**B**) ErbB-RASER1C-dCas9VP64 and a TRE3G-directed sgRNA activate TRE3G-mCherry in an ErbB activity-dependent manner in BT-474 cells. mTurquoise is marker for gRNA expression. Scale bar, 100 μm. (**C**) Quantification of (B). AU, arbitrary units. NS, not significant. Differences between conditions were assessed by the Kruskal-Wallis test followed by two-tailed Dunn's posthoc tests. $p = 6.5 \times 10^{-8}$ for the overall null hypothesis of no difference between groups (n = 50 randomly selected transfected cells). (**D**) Schematic of the ErbB-RASER1C-dCas9VP64 system regulating endogenous GM-CSF. (**E**) RASER activates endogenous GM-CSF in ErbB-hyperactive cells. LN-229:EGFRvIII cells expressing constitutively active ErbB1 and MCF-7 cells with normal ErbB were transfected with ErbB-RASER1C-dCas9VP64, GM-GSF gRNA containing MS2-binding sequences, and MS2-p65-HSF1 (MPH). After 24 h, released GM-CSF was quantified by ELISA (n = 3 biological replicates). (**F**) Induction of GM-CSF protein by RASER1C-dCas9VP64 is > 4-fold more efficient in LN-229:EGFRvIII cells than in ErbB-normal MCF-7 cells (n = 3 biological replicates). All error bars represent s.e.m.

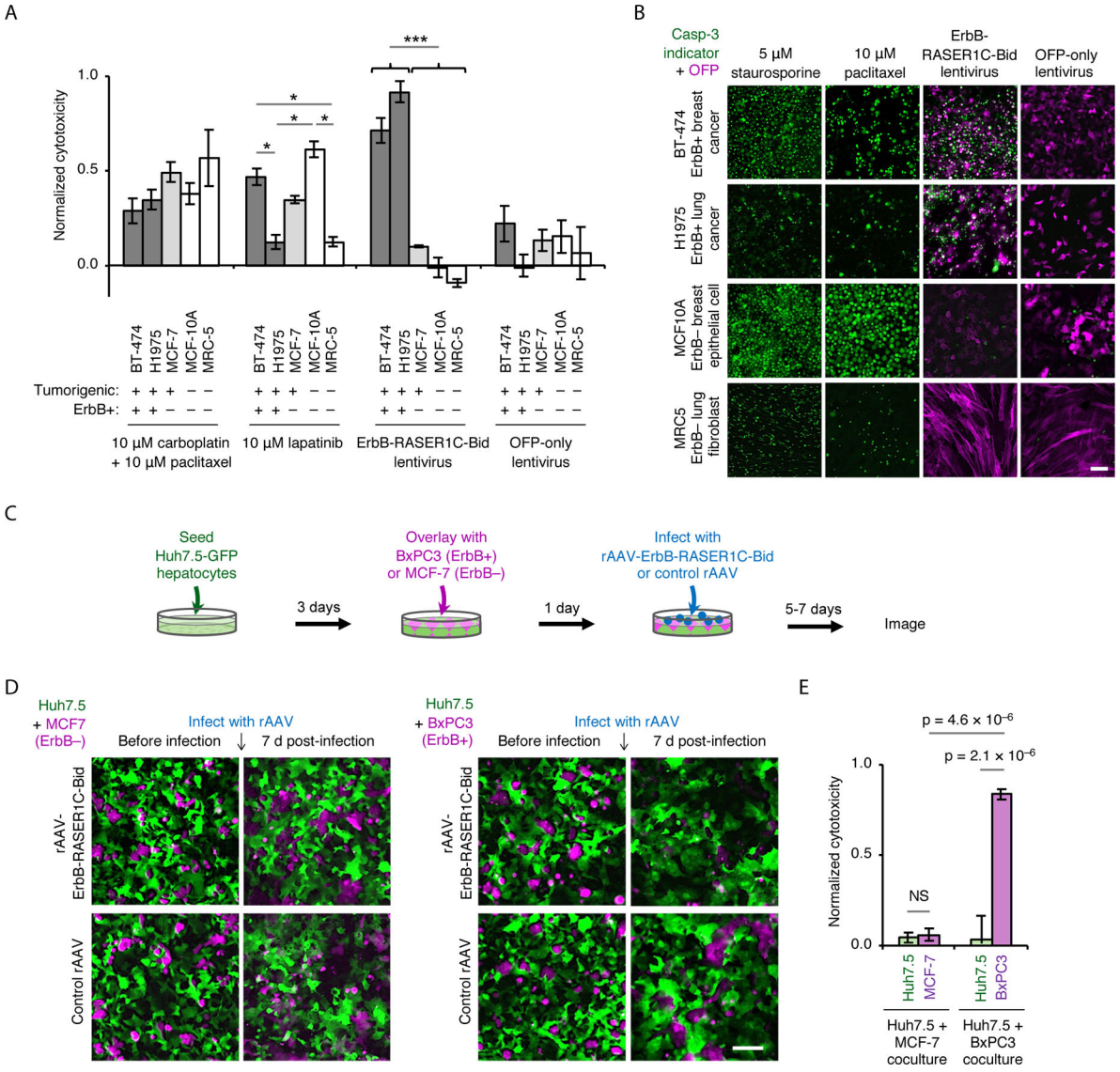

Fig. 6.

RASER as an anti-cancer agent. (**A**) Cytotoxicity of conventional antitumor agents and ErbB-RASER1C-Bid lentivirus in ErbB-hyperactive cancer cell lines (BT-474 and H1975) or ErbB-normal cell lines (MCF-7, MCF-10A and MRC5). Cell viability was measured by fluorescence of the live cell marker Gly-Phe-AFC, then converted to cytotoxicity. Error bars represent s.e.m., n = 6 (BT-474, MCF-10A) or 3 (MCF-7, H1975, MRC-5). *$p < 0.05$ for indicated comparisons, ***$p < 0.001$ for all comparisons between ErbB+ and ErbB− cells. (**B**) Cells were treated with paclitaxel, ErbB-RASER1C-Bid lentivirus, or OFP-only lentivirus. Staurosporine is a positive control for apoptosis. Apoptosis was detected using a caspase-3 fluorescent indicator (green), and infected cells were detected by OFP (magenta). In BT-474 and H1975 cells, apoptosis is induced to higher levels by the RASER virus than by paclitaxel. In MCF10A and MRC5 cells, apoptosis is induced by paclitaxel but not by the RASER virus. Scale bar, 100 μm. (**C**) Testing AAV-ErbB-RASER1C-Bid specificity in a co-culture model of disseminated disease. Normal ErbB Huh7.5-GFP were differentiated by 1%

DMSO treatment for 4 days. Cell tracker orange labeled BxPC3 (ErbB-hyperactive pancreatic cancer) or MCF7 (ErbB-normal) were co-cultured with Huh7.5-GFP monolayer for 24 h. rAAV-RASER1C-Bid and control rAAV were infected at the specified multiplicity of infection (MOI). Cells were imaged and counted 5–7 days later. (**D**) Co-cultures were infected by rAAV-ErbB-RASER1C-Bid or control rAAV at MOI 3×10^6 and imaged 7 days later. Scale bar, 100 μm. (**E**) Quantification of cell cytotoxicity from (D). Cell numbers from AAV-RASER1C-Bid infection were subtracted from the cell numbers of control AAV infection, than normalized to control (n = 6 for Huh7.5 + MCF-7, n = 7 for Huh7.5 + BxPC3, error bars represent s.e.m). Only ErbB-RASER target, BxPC3 cells show a significant reduction ($p < 3.7 \times 10^{-6}$) while no significant difference in ErbB− cells, Huh7.5 and MCF7. All statistical significance was tested by one-way ANOVA followed by Holm-Sidak's multiple comparisons test.